Communications in Physics, Vol. 31, No. 4 (2021), pp. 343-352
DOI:https://doi.org/10.15625/0868-3166/15702

INVESTIGATION OF SHAPE MEMORY EFFECT IN NI-TI BASED ALLOYS

NGUYEN HUY DAN[1,2,†], KIEU XUAN HAU[1], NGUYEN HAI YEN[1,2],
PHAM THI THANH[1,2], NGUYEN HUY NGOC[1,2], DANG DOAN NUOI[1]
AND TRAN DANG THANH[1,2]

[1]*Institute of Materials Science, Vietnam Academy of Science and Technology, 18 Hoang Quoc Viet, Hanoi, Vietnam*

[2]*Graduate University of Science and Technology, Vietnam Academy of Science and Technology, 18 Hoang Quoc Viet, Hanoi, Vietnam*

E-mail: [†]dannh@ims.vast.ac.vn

Received 26 November 2020
Accepted for publication 7 June 2021
Published 15 September 2021

Abstract. *Shape memory alloys (SMAs) are capable of many applications in the fields of biomedical, aerospace, microelectronics, automation, for examples, orthodontics, stents, bone anchors, automatic valves, heat sensors, nanotweezers, robots... In this paper, we present an overview of current research of SMAs and our initial results obtained on Ni-Ti based alloys of Ni-Ti, Ni-Ti-Zr-Cu-Cr, Ni-Ti-Zr-Cu-Co, Ni-Ti-Zr-Cu-Nb and Ni-Ti-Zr-Cu-Hf prepared by melt-spinning method. The existence of martensitic phases with B19' structure type and austenitic phases with B2 structure type at room temperature depends on the composition of the alloys. The structural transformation from B19' to B2 in the temperature range of 60-80°C has been observed by high-temperature XRD patterns and DSC curves. With addition of Zr, Cu, Cr, Co, Nb and Hf elements, the structural transformation in Ni-Ti based alloys happens at higher temperature, in regions of 500 - 650°C. The B19'-R-B2 intermediate transformation has been observed in the Ni-Ti-Zr-Cu-Cr sample. The shape memory effect of some samples were directly examined.*

Keywords: shape memory effect; shape memory alloy; high entropy alloy; structural transformation; melt-spinning method.

Classification numbers: 62.20.fg.

I. INTRODUCTION

Shape memory effect (SME) was first discovered in 1932 by Ölander on Au-Cd alloy [1]. This alloy can be plastically deformed when cooled and recovers to its original shape when it is heated. With the concentration of Cd in range of 46.5 - 50%, the Au-Cd alloy has the transformation temperature from 30 to 100˚C. Later, a series of other shape memory alloys (SMAs) were manufactured such as Cu-based alloys (Cu-Zn, Cu-Sn), Ni-based alloys (Ni-Ti, Ni-Al), Fe-based alloys (Fe-Pd, Fe-Pt) [2–30]. However, the most commonly used SMAs are nitinol alloys (Ni-Ti) and Heusler alloys (Cu-Ni-Al, Ni-Mn-Ga) [16-30]. Recently, the SME has been observed on some high entropy alloys (HEAs) such as Ti-Ta-Hf-Nb-Zr, Fe-Ni-Co-Al-Ti, Ti-Zr-Co-Ni-Cu. The combination of preeminent features of SMA and HEA (high strength, heat resistance, low diffusion coefficient) will provide helpful applications in practice [16].

The SME in Ni-Ti alloys was first reported in 1963 [17]. In the process of studying Ni-Ti alloys, the basic properties, including superplastic features, have been greatly improved. The Ti-Ni alloys not only possess a good SME, mechanical and corrosion resistance but also have high biological compatibility. Therefore, they have been widely used in industrial and biomedical fields [14–21]. Although widely used in the past few decades, Ni-Ti alloys have shown some disadvantages that prevent the expansion of their applications in practice. These are bad deformation at low temperature, high material cost, slow reaction to temperature change, small operating temperature range and poor repeatability [14–16]. Besides, high concentrations of Ni in the alloys can also causes allergies to the human body leading to limitations in biological applications. Therefore, some researchers have added other elements (Cu, Zr, Nb, Ta...) into Ni-Ti alloys and changed the manufacturing technology conditions to minimize the disadvantages of these alloys [14–16, 19–21]. The addition of other elements causes the change of transformation temperature and the transformation from β to α type of martensitic phase (orthorhombic structure). On the other hand, the SME of the alloys is simultaneously improved. So far, many types of Ni-Ti SMAs have been manufactured with high biological compatibility and plastic deformation.

The SME in Cu-Al-Mn Heusler alloys was first published in 1996 [22]. The superelasticity (SE) of these alloys is improved through controlling structure and particle size [23–31]. So far, the superelastic property of these alloys has reached the level of Ni-Ti ones. Because of their high ductility, they are easily deformed (by rolling, drawing, punching methods) to form more complicated shapes than Ni-Ti alloys. These alloys were used in medical devices and began to be commercialized in 2012 [32]. In conventional SMAs, including Ti-Ni alloys, when both the strain and stress induced by SME are very large, the response to the input signal is very low, below 10 Hz. That is because the deformation of the material is controlled by changing the temperature [33]. Therefore, the research for new SMAs, whose SME is caused by factors other than temperature, such as magnetic field, is essential. In 1996, the SME affected by the magnetic field (Magnetic shape memory effect - MSME) was first studied by Ullakko et al. on Ni_2MnGa Heusler alloy [34]. Although studies showed that a strain greater than 10% was caused by an external magnetic field, the Ni-Mn-Ga alloys have not been used in practice because of their brittleness, high cost and low work output stress (below 5 Mpa). In 2006, a new type of Heusler magnetic SMA, (Ni, Co)-Mn-In alloys, could solve the problems of brittleness and low output stress [35–37]. The (Ni, Co)-Mn-In alloys show a phase transformation from ferromagnetic austenite phase (FM) to paramagnetic martensite phase (PM) and thermodynamic stability of the FM phase increased via Zeeman energy

affected by the external magnetic field in a certain temperature range. At a fixed temperature, the SME can be obtained by using the magnetic phase transition process when an external magnetic field is applied. The (Ni, Co)-Mn-In alloys can recover the almost perfect shape of deformation of about 3% by using static or pulsed magnetic field with a strength of 70 kOe [37]. These SMAs are called magnetic SMAs (Magnetic shape memory alloy - MSMA) because their SME is caused by magnetic phase transition. The study results were published with other Ni-Mn-based Heusler alloys, such as (Ni, Co)-Mn-Sn [38], indicating that the output stress of these MSMAs is almost proportional to the strength of the applied magnetic field and it can be greater than 100 MPa [39]. In addition, a reverse magnetocaloric effect (the material is cooled under an applied magnetic field) was also detected in MSMAs [40, 41]. The mechanisms of changes of structure, magnetic properties, stress and strain of these alloys under the impact of the external magnetic field have been greatly studied. However, the processes that occur in the MSMAs under an applied magnetic field are not fully understood.

Recently, to expand the scope of applications, the multi-component SMAs have been concentratedly studied. The Fe-based superelastic MSMAs of Fe-Ni-Co-Al-Ta-B [42] and Fe-Mn-Al-Ni [43] were published in 2011 and 2013, respectively. The superelasticity is obtained by the transformation of martensite phase from α (bcc) to γ (fcc) in Fe-Mn-Al-Ni alloys and from γ (fcc) to α' (bct) in Fe-Ni-Co-Al-Ta-B alloys. The Fe-Ni-Co-Al-Ta-B alloy exhibits superelastic deformation of about 13% and high-stress hysteresis. However, the ductility and superelasticity of the alloy are greatly reduced during the sample machining process. When rolled into thin sheets, the superelasticity of the alloy decreases by more than 95%. Therefore, it is difficult to make these alloys in wire form and still retain their superelasticity. This limits the practical applications of the Fe-Ni-Co-Al-Ta-B alloys [42]. As for the Fe-Mn-Al-Ni alloys, one of the most important features is their extremely small dependence of the critical stress on temperature. This is because the transformation entropy change is about 10 times smaller than that of Ni-Ti alloys [43]. This means the temperature range for superelasticity in the Fe-Mn-Al-Ni MSMAs is 10 times greater than that of the Ti-Ni SMAs. This feature makes it useful for applications in the automotive and aerospace industry because of the huge temperature changes in those applications. The superelasticity of the Fe-Mn-Al-Ni MSMAs is greatly affected by the shape and size of particles in the alloys [43]. Therefore, changing the manufacturing technology conditions to obtain the optimal particle structure for this type of MMSAs is necessary [44–46]. Recently, some scientists have discovered SME on some high entropy alloys such as Ti-Ta-Hf-Nb-Zr, Ti-Zr-(Co, Hf)-Ni-Cu… [47, 48]. The combination of preeminent features of shape memory and high entropy alloys (high durability, heat resistance, low diffusion coefficient…) will provide potential applications in practice.

In this work, we give an overview of current research of shape memory alloys and our obtained initial results of Ni-Ti based alloys of Ni-Ti, Ni-Ti-Zr-Cu-Cr, Ni-Ti-Zr-Cu-Co, Ni-Ti-Zr-Cu-Nb and Ni-Ti-Zr-Cu-Hf prepared by using melt-spinning method.

II. EXPERIMENT

The samples were prepared by using the melt-spinning method. First, elements of Ni, Ti, Zr, Cu, Cr, Co, Nb and Hf with their purity of 99.9% are determined by the molar concentration (Table 1). An arc-melting method was performed to ensure the homogeneity of alloys. These alloys are then used as input materials for the melt-spinning method with tangential velocity of copper roller of 40 m/s. The obtained ribbons have the width of about 3 mm and the thickness of

about 30 μm. The samples, symbolized in Table 1, correspond to the molar concentration of the elements in the sample. The structural characteristic and structural transformation were analyzed by an X-ray diffractometer (Equinox 5000-Thermo Scientific) with the Cu-K_α radiation source ($\lambda = 1.5406$) at room temperature and high temperature in vacuum. The transformation temperature and the activation energy of the samples were studied by differential scanning calorimetry (DSC) on Labsys Evo 1600-SETARAM apparatus. The SME of the alloy ribbons is observed by bending them at room temperature and then placing them on a flat furnace with a temperature indicator. When the temperature increases, the alloy ribbons are straighten back to their original shape. By observing the temperature and shape change, we can determine the temperature and amplitude of the shape memory effect of the alloy ribbons. All measurements are performed in the direction of increasing temperature.

Table 1. Symbol and percentage of the molar concentration of the elements in the samples (with A = Cr, Co, Nb, Hf).

Symbol	Ni	Ti	Zr	Cu	A
S1	51	49	0	0	0
S2	50	50	0	0	0
S3	49	51	0	0	0
S4	25	50/3	50/3	25	50/3 (Cr)
S5	25	50/3	50/3	25	50/3 (Co)
S6	25	50/3	50/3	25	50/3 (Nb)
S7	25	50/3	50/3	25	50/3 (Hf)

III. RESULTS AND DISCUSSION

According to the review report by Chekotu *et al.* [49], there are three different structural transformations in the NiTi based alloy system. In the martensitic phase, NiTi alloy has a low symmetrical structure corresponding to the B19' structure type. In the austenitic phase, NiTi alloy has a face-centered cubic lattice structure with high symmetry corresponding to the B2 structure type. The martensitic phase is characterized by needle-like crystals arranged in a herringbone shape. The austenitic phase usually has a high hardness, while the martensitic phase is softer, more malleable and lower stress. In some cases, the intermediate R-phase with a rhombic structure has low transformation strain and low thermal hysteresis. The R-phase can occur in Ni-rich alloys or due to the addition of some other elements into the alloy such as Fe [50].

Figure 1 shows XRD patterns of the obtained ribbons measured at room temperature. It is visible that the S1 sample has two main diffraction peaks at 2θ angular corresponding to 44° and 62° (Figure 1a). These diffraction peaks corresponding to the B2 phase (ICDD PDF 00-018-0899) belong to the cubic system with a lattice constant of a $\sim$ 2.99 Å (the space group Pm3m). Meanwhile, the S2 and S3 samples have B19' structure type (ICDD PDF 00-027-0344), belongs to the monoclinic system (a $\sim$ 2.89 Å; b $\sim$ 4.12 Å; c $\sim$ 4.62 Å and $\beta \sim 96.8°$), the space group P21/m. Both the B2 and B19' phases are common structural phases in the martensite phase [49, 51].

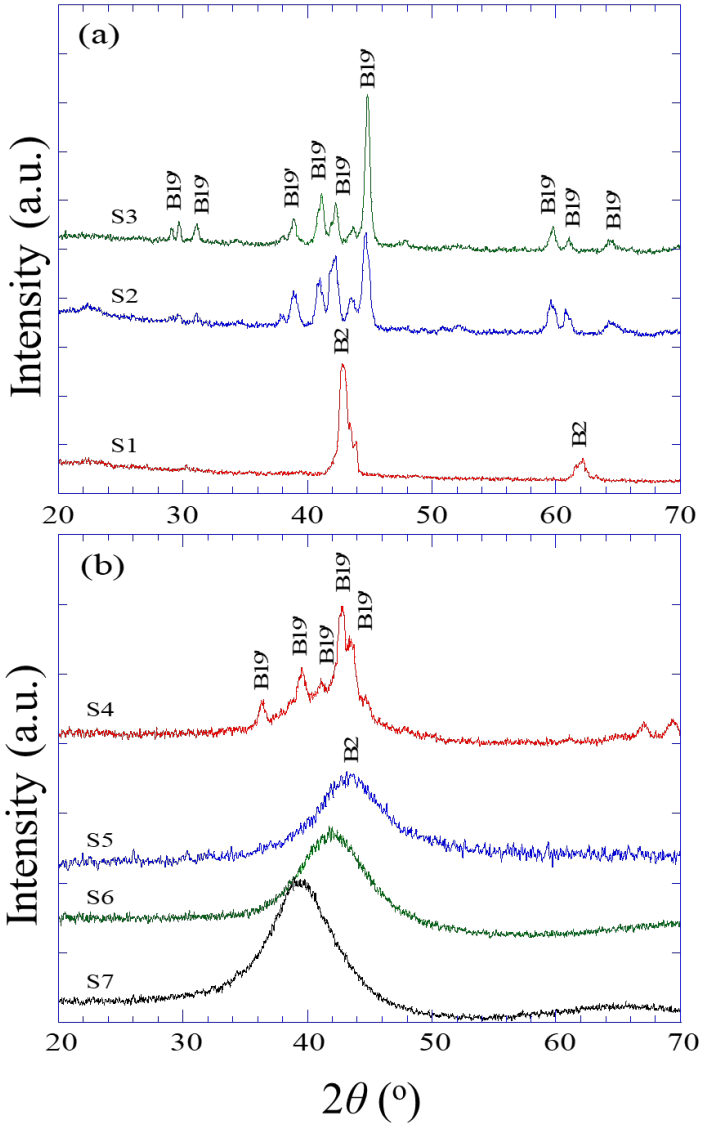

Fig. 1. XRD patterns of the obtained alloy ribbons measured at room temperature.

As shown in Fig. 1b, the S4 sample has a coexistence of both the B2 and B19' phases. Meanwhile, the S5, S6 and S7 samples only show the characteristics of the B2 phase. The characteristic peak of the B2 phase in the S4-S7 samples has a completely different shape compared to the S1 sample. It is possible that the B2 phase in these samples exists in nanocrystalline form. However, the characteristic diffraction peaks for the B2 phase of S4, S5, S6 and S7 shift to lower 2θ angle corresponding to A = Cr, Co, Nb and Hf, respectively. The shift of B2 diffraction peak is attributed to the increase in the atomic radius of the Cr, Co, Nb and Hf added elements in the alloy. The addition of Zr, Cu, Cr, Co, Nb and Hf to the alloy not only changes the lattice constant,

improves the mechanical properties but also creates high entropy alloy systems that have a large SME in the high-temperature range [52, 53]. Fig. 2 shows the DSC curves of the S2, S4, S5 and S6 samples measured with increasing temperature. It can be seen that the DSC curves of these samples display exothermic peaks. These exothermic peaks occur at temperatures of 65˚C; 505˚C; 624˚C and 632˚C for the S2, S4; S5 and S6 samples, respectively.

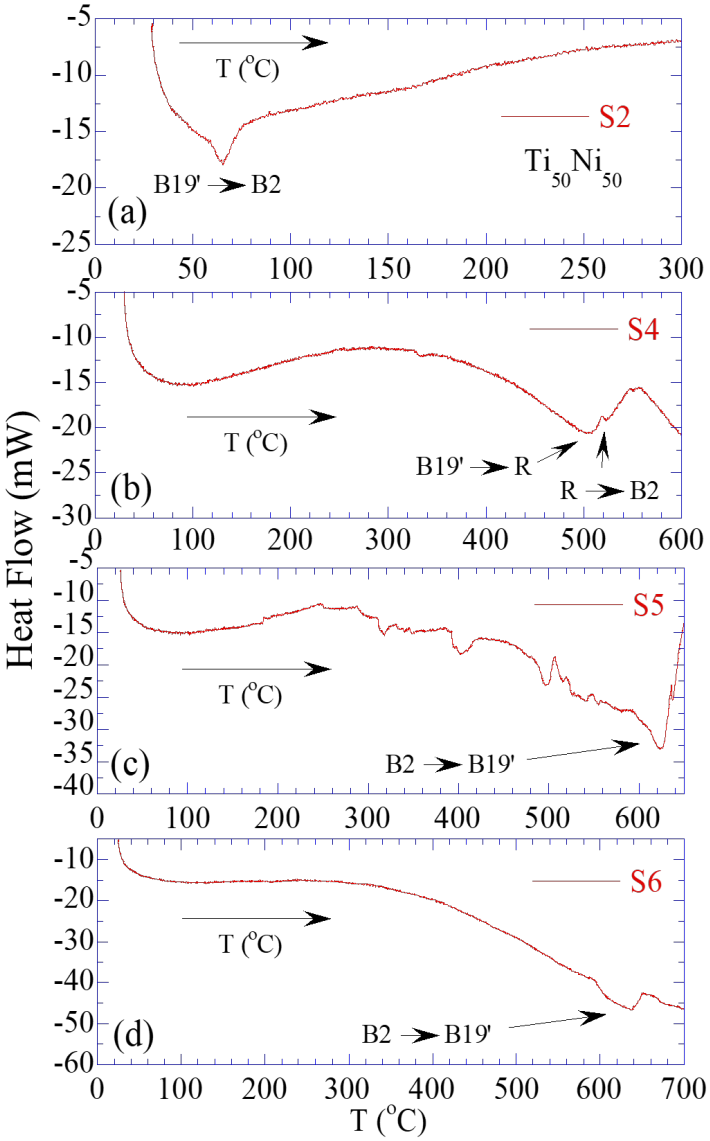

Fig. 2. DSC curve of S2 (a), S4 (b), S5 (c) and S6 (d) samples measured at increasing temperature.

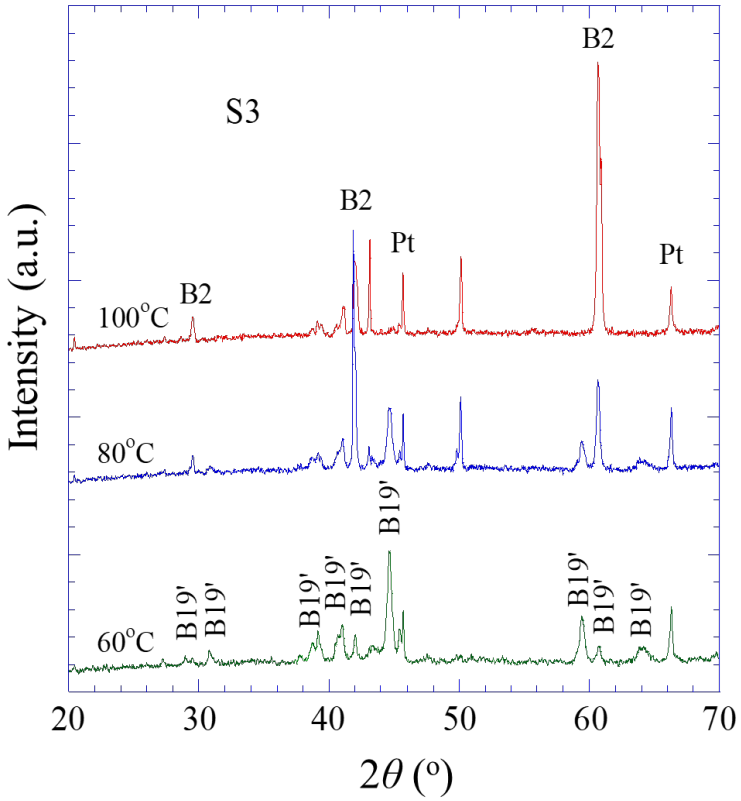

Fig. 3. XRD pattern of S3 sample measured at 60, 80 and 100˚C.

Figure 3 shows an XRD pattern of the S3 sample at temperatures of 60, 80 and 100˚C. In this experiment, the alloy ribbons are glued onto a Pt bar with a conductive adhesive. The Pt bar plays a role as a heater which is used to increase the temperature of the sample. Therefore, the XRD patterns of the alloy ribbons appear the characteristic diffraction peaks of Pt. In the temperature range below 60˚C, we have not observed any change in the XRD pattern of the material. This means that the B19‘ structure is stable in the temperature range below 60˚C. However, when the temperature of the sample is higher than 60˚C, new diffraction peaks with strong intensity appear at the angle of 29.5, 42 and 61˚. These peaks correspond to the B2 phase as discussed above. This means that the crystal structure transformation of the material will be occurred in the temperature range from 60˚C to 80˚C. From the results of DSC analyses and XRD patterns, we see that the observed exothermic peak at 65˚C on the DSC curve of the S2 sample is a characteristic related to the structural phase transformation from B19‘ to B2. These results are in good agreement with the obtained results by Swiec *et al.* [52] when studying the structural phase transformation in the NiTi alloy system.

It is quite interesting that with the addition of Zr, Cu, Cr, Co, Nb and Hf elements to the NiTi based alloy, we observed the signals related to structural phase transformations in the high-temperature region (about 500-650˚C). In detail, the structural phase transformations from B19’

to R at 505˚C, then from R to B2 at 525˚C, are occurred in the S4 sample. The structural phase transformations of B2 to B19' at 624˚C and 632˚C corresponding to S5 and S6 samples, respectively, are determined. The elements Zr, Cu, Cr, Co, Nb and Hf are selected for adding to the alloy because they are easy to form high entropy alloys. This is a desirable property to increase applicability of SME of the alloys. These elements can also increase the glass forming ability (reduce crystallinity) and increase the structural transformation temperature (the temperature where SME occurs) to the higher temperature range for the alloy. The XRD analysis results show that Co, Nb and Hf increase the glass forming ability of the alloy stronger than Cr. The elevation of the structural transformation temperature to the high temperature region of the elements of Cr, Co and Nb is shown by DSC analysis and this ability increases from Cr to Nb, respectively.

According to Frenzel *et al.* [54], the change in Ni concentration in the alloy significantly affects to the stress required for martensitic transformation and deformation recovery. Therefore, the influence of the composition ratio of the elements in the alloy on the structure, SME and their mechanical properties is a subject that needs to be studied more carefully [55, 56].

Thus, the above research results show that the samples are heated to a certain temperature leading to martensitic-austenitic structure transformation in the material. This is the basis of shape memory alloy systems. Therefore, this shape memory effect is also called as the heat memory effect [55]. To verify the SME of the fabricated samples, we select some typical samples including the S1, S2 and S3 samples. Initially, the samples are flat at room temperature. We applied a force to deform them. The deformed samples were placed on a heater to increase their temperature. A change in the shape of the sample at a corresponding temperature has been recorded. For the S4-S8 samples, due to their high structural transformation temperature (> 500˚C), specialized equipment is required to observe their shape transformation at high temperatures.

IV. CONCLUSION

Some Ni-Ti based alloys have been fabricated and studied for their structural characteristics, shape memory effect. The obtained results showed the existence of martensitic phases with B19' structure type and austenitic phases with B2 structure type. The structural transformation from B19' to B2 in the temperature range of 60-80˚C has been observed by high-temperature XRD patterns and DSC curves. By adding the Zr, Cu, Cr, Co, Nb and Hf elements, we have obtained Ni-Ti based alloys that have structural transformation temperature at higher temperature regions (about 500-650˚C). The signal of the B19'-R-B2 intermediate transformation in the S4 sample (with doping of Zr, Cu and Cr) was observed. The shape memory effect of some samples has been directly examined when they were heated.

ACKNOWLEDGMENTS

This work was supported by the National Foundation for Science and Technology Development (NAFOSTED) of Viet Nam under grant number of 103.02-2019.344. A part of the work was done in the Key Laboratory for Electronic Materials and Devices, IMS-VAST.

REFERENCES

[1] A. Ölander, *Am. Chem. Soc.* **54** (1932) 3819.
[2] J. Xia, T. Omori and R. Kainuma, *Scripta Mater.* **187** (2020) 355.
[3] J. M. Vallejos, M. F. Giordana, C. E. Sobrero and J. A. Malarria, *Scripta Mater.* **179** (2020) 25.

[4] B. Pricop, A. U. Söyler, B. Özkal and L. G. Bujoreanu, *Front. Mater.* **7** (2020) 1.
[5] E. Clithy, *Sci Insigt.* **33** (2020) 167.
[6] C. Yang, S. Abanteriba and A. Becker, *AIP Advances* **10** (2020) 060701.
[7] Y. Shen, Z. Wei, W. Sun, Y. Zhang, E. Liu and J. Liu, *Acta Mater.* **188** (2020) 677.
[8] M. L. Lapér, R. Guimarães, B. R. Barrioni, P. A. P. Silva, M. Houmard, E. M. Mazzer and E. H. M. Nunes, *J. Mater. Res. Technol.* **9** (2020) 3676.
[9] A. Agrawal and S. K. Vajpai, *Mater. Sci. Technol.* **36**(12) (2020) 1337.
[10] N. S. Al-Humairi, S., *Cu-Based Shape Memory Alloys: Modified Structures and Their Related Properties*, Recent Advancements in the Metallurgical, (2020).
[11] M. M. Pan, X. M. Zhang, D. Zhou, R. D. K. Misra and P. Chen, *Mater. Sci. Eng. A* **797** (2020) 140107.
[12] W. Abuzaid and H. Sehitoglu, *Scripta Mater.* **169** (2019) 57.
[13] A. Walnsch, M. J. Kriegel and O. Fabrichnay, A. Leineweber, *J. Phase Equilib. Diffus* **41** (2020) 457.
[14] R. L. Soares and W. B. de Castro, *Int. Eng. J.* **72** (2019) 227.
[15] K. Otsuka and C. M. Wayman, *Shape Memory Materials*, Cambridge University Press, 1998.
[16] R. Kainuma, *Mater. Trans.* **59** (2018) 327.
[17] W. J. Buehler, J. V. Gilfrich and R. C. Wiley, *J. Appl. Phys.* **34** (1963) 1475.
[18] H. Huang, Y. Z. Zhu and W. S. Chang, *Adv. Mater. Sci. Eng.* **2000** (2020) 8024803.
[19] Y. Tong, A. Shuitcev and Y. Zheng, *Adv. Eng. Mater.* **22** (2020) 1900496.
[20] H. Y. Lu, C. H. Chen and N. T. Tsou, *Materials* **12** (2019) 57.
[21] S. Dhala, S. Mishra, A. Tewari and A. Alankar, *Int. J. Plast.* **115** (2019) 216.
[22] R. Kainuma, S. Takahashi and K. Ishida, Metall. Mater. Trans. A **23** (1996) 2187.
[23] A. P. Kamantsev, Yu. S. Koshkid'ko, E. O. Bykov, V. S. Kalashnikova , A. V. Koshelev, A. V. Mashirova, I. I. Musabirovh, M. A. Paukov and V. V. Sokolovskiy, *Phys. Solid State* **62** (2020) 815.
[24] C. Seguí, J. Torrens-Serra, E. Cesari and P. Lázpita, *Materials* **13** (2020) 419.
[25] X. Wang, M. Wu, T. Yang and R. Khenata, *RSC Adv.* **10** (2020) 17829.
[26] T. Kihara, X. Xu, A. Miyake, Y. Kinoshita, M. Tokunaga, Y. Adachi and T. Kanomata, *Scripta Mater.* **181** (2020) 25.
[27] M. Alizadeh and M. Avazzadeh, Materials Science & Engineering A **757** (2019) 88.
[28] Z. Wei, Y. Shen, Z. Zhang, J. Guo, B. Li, E. Liu, Z. Zhang and J. Liu, *APL Mater.* **8** (2020) 051101.
[29] T. Bachaga, J. Zhang and M. Khitouni, *Int. J. Adv. Manuf. Tech.* **103** (2019) 2761.
[30] X. Xu, T. Kanomata, N. Yamazaki, H. Nishihara, M. Nagasako, Y. Adachi, T. Sakon, R. Kainuma, *J. Alloys Compd.* **785** (2019) 484.
[31] S. Xu, R. Tsukuda, M. Zhao, X. Xu, T. Omori, K. Yoshimi and R. Kainuma, Scripta Materialia **177** (2020) 74.
[32] T. Tanaka, S. Kise, T. Omori, R. Kainuma and K. Ishida, Materia (Rio J.) **51** (2012) 108.
[33] J. M. Jani, M. Leary, A. Subic and M. A. Gibson, *Mater. Des.* **56** (2014) 1078.
[34] K. Ullakko, J. K. Huang, C. Kantner, R. C. O. Handley and V.V. Kokorin, *Appl. Phys. Lett.* **69** (1996) 1966.
[35] R. Kainuma, Y. Imano, W. Ito, Y. Sutou, H. Morito, S. Okamoto, O. Kitakami, K. Oikawa, A. Fujita, T. Kanomata and K. Ishida, *Nature* **439** (2006) 957.
[36] I.N. Glavatskyy, O. Glavatska, S.P. Söderberg, Hannula and J.U. Hoffmann, *Scripta Mater.* **54**(11) (2006) 1891.
[37] T. Sakon, S. Yamazaki, Y. Kodama, M. Motokawa, T. Kanomata, K. Oikawa, R. Kainuma and K. Ishida, *Jpn. J. Appl. Phys.* **46** (2007) 995.
[38] R. Kainuma, Y. Imano, W. Ito, H. Morito, Y. Sutou, K. Oikawa, A. Fujita, K. Ishida, S. Okamoto, O. Kitakami and T. Kanomata, *Appl. Phys. Lett.* **88** (2006) 192513.
[39] H.E. Karaca, I. Karaman, B. Basaran, Y. Ren, Y.I. Chumlyakov and H.J. Maier, *Adv. Funct. Mater.* **19** (2009) 983.
[40] T. Krenke, E. Duman, A. Acet, E.F. Wassermann, X. Moya, L. Manosa and A. Planes, *Nat. Mater.* **4** (2005) 450.
[41] Y. Tanaka, Y. Himuro, R. Kainuma, Y. Sutou, T. Omori and K. Ishida, *Science* **327** (2010) 1488.
[42] T. Omori, K. Ando, M. Okano, X. Xu, Y. Tanaka, I. Ohnuma, R. Kainuma and K. Ishida, *Science* **333** (2011) 68.
[43] T. Omori, M. Okano and R. Kainuma, *APL Mater.* **1** (2013) 032103.
[44] X. Huang and Y. Liu, *Scr. Mater.* **45** (2001) 153.
[45] B. Cao and T. Iwamoto, *EPJ Web of Conferences* **183** (2018) 02025.

[46] M. Vollmer, T. Arold, M. J. Kriegel, V. Klemm, S. Degener, J. Freudenberger and T. Niendorf, *Nat. Commun.* **10** (2019) 2337.
[47] Y. Iijima, T. Nagase, A. Matsugaki, P. Wang, K. Ameyama and T. Nakano, *Mater. Des.* **202** (2021) 109548.
[48] D. Canadinc, W. Trehern, J. Ma, I. Karaman, F. Sun and Z. Chaudhry, *Scripta Mater.* **158** (2019) 83.
[49] J. C. Chekotu, R. Groarke, K. O'Toole and D. Brabason, *Materials* **12** (2019) 809.
[50] A. Motallebzadeh, M. B. Yagci, E. Bedir, C. B. Aksoy, D. Canadinc, *Metall. Mater. Trans. A* **49** (2018) 1992.
[51] C. Hayrettin, O. Karakoc, I. Karaman, J.H. Mabe, R. Santamarta and J. Pons, *Acta Mater.* **163** (2019) 1.
[52] P. Swiec, M. Zubko, Z. Lekston, D. Stroz, *Proceeding of the XXIII Conference on Applied Crystallography*, Krynica Zdroj, Poland, **9** (2015) 20.
[53] S. Dadbakhsh, M. Speirs, J. van Humbeeck and J.P. Kruth, *MRS Bull.* **41** (2016) 765.
[54] J. Frenzel, E. P. George, A. Dlouhy, C. Somsen, M. F. X. Wagner and G. Eggeler, *Acta Mater.* **58** (2010) 3444.
[55] S. Saedi, A.S. Turabi, M.T. Andani, N.S. Moghaddam, M.H. Elahinia, H.E. Karaca, *Mater. Sci. Eng.* **686** (2017) 1.
[56] F. X. Li, P. D. Hao, J. H. Yi, D. Şopu, J. Tan, X. Y. Chong, J. Eckert, *Intermetallics* **98** (2018) 60.